RSC Advances

PAPER

View Article Online
View Journal | View Issue

Cite this: *RSC Adv.*, 2024, **14**, 28779

$Li_4Ti_5O_{12}$@carbon nanotube arrays as high-performance anode for Li-ion batteries†

Bin Zhu, Yi Pu, Wu Tang* and Hui Tang *

Received 17th June 2024
Accepted 1st September 2024

DOI: 10.1039/d4ra04421e

rsc.li/rsc-advances

The innovation of advanced high-rate anodes is of great significance for the development of high-power and fast-charging lithium-ion batteries (LIBs). In this work, self-supported $Li_4Ti_5O_{12}$@carbon (LTO@C) nanotube arrays as a high-quality anode are fabricated *via* anodizing and hydrothermal processes. Owing to the structure having a high contact surface area and good stability, as well as the incorporation of carbon, the LTO@C exhibits a remarkable rate capability (a reversible capability of 290 mA h g^{-1}, 251.9 mA h g^{-1}, 228.8 mA h g^{-1}, and 208.7 mA h g^{-1} at 1C, 5C, 10C, and 20C, respectively) and cycling performance (71.7% capacity retention after 1000 cycles at 10C), which is superior to LTO. These features suggest the promising application of LTO@C in high-power energy storage areas.

Introduction

In the past few decades, owing to their high power density and long cycle life, lithium-ion batteries (LIBs) have dominated the battery market. However, the long charging time of LIBs is a significant obstacle for new energy electric vehicles.[1] To meet the rapidly growing demand for vehicle batteries, the exploration of high-energy-density and fast charging electrode materials is essential.[2,3] Commercial graphitic carbon commonly used as anodes in LIBs often suffers from a low lithium diffusion coefficient and the formation of a solid electrolyte interphase (SEI) film, leading to poor rate performance and serious safety issues.[4–6] Compared to carbon anodes, spinel-type lithium titanate ($Li_4Ti_5O_{12}$, LTO) anodes have garnered more attention due to their high lithiation potential (1.55 V *vs.* Li/Li^+), zero-strain feature, and low-reactivity with common inorganic electrolytes.[7,8] These advantageous properties prevent lithium deposition and facilitate fast lithium ion (Li+) (de-)intercalation, making LTO a popular choice for anodes in LIBs. Nonetheless, the unsatisfactory rate capability due to LTO's poor electrical conductivity (10^{-13} S cm^{-1}) remains a significant issue that must be addressed for its application in high-power devices.[9–11]

To address these issues, several strategies have been employed, such as downsizing the LTO particle sizes to the nano-regime[12,13] and surface modifications, particularly carbon coatings.[14–17] Among these, constructing a carbon coating layer on the surface of LTO has been considered the most effective approach. Cao *et al.*[6] used $TiO(acac)_2$ as both the titania and carbon source to synthesize $Li_4Ti_5O_{12}$/carbon core–shell electrodes, resulting in high-power performance due to its fast kinetics for both transported Li^+ ions and electrons. In another report, polypyrrole was utilized as a pivotal carbon and nitrogen source to obtain a self-assembled *N*- and anatase-TiO_2 doped $Li_4Ti_5O_{12}$/C nanorod material. The obtained anode exhibited a high rate capacity of 196.3 mA h g^{-1} at 0.5C and 105.5 mA h g^{-1} at 100C.[18] Similarly, Peng *et al.*[19] used a simple solid-phase sintering method to fabricate carbon-coated LTO, using TiO_2 particles and lithium carbonate as precursors. These approaches simplify the synthesis processes of carbon-coated LTO without requiring complicated multistep procedures. However, these materials inevitably need to be mixed with a binder and conductive agent before being used in LIBs, which introduces undesirable interfaces and limits the overall specific capacity.

Therefore, constructing binder-free arrays is an effective method to overcome the aforementioned drawbacks in preparing high-performance LTO anodes. Anodization is a proficient technique for synthesizing uniform titanium dioxide nanotube arrays. In recent years, the TiO_2-based nanotube arrays fabricated by anodization have been used as high-performance anodes.[20–23] The choice of carbon coating source is crucial. Instead of popular commercial carbon materials such as Ketjen black, graphene, and carbon nanotubes, low-cost, more commonplace sucrose and glucose were used as carbon sources to form the carbon coating.[10,24]

Herein, we construct hierarchical LTO@C nanotube arrays through anodization followed by a rational hydrothermal route utilizing low-cost glucose as the carbon source. Additionally, the forming of LTO and carbon coating is accomplished *via* a one-step hydrothermal process. The LTO@C combines the hollow structure of nanotubes with a carbon layer coating. The obtained hollow structure enhances the transfer of Li^+, while the

School of Materials and Energy, University of Electronic Science and Technology of China, Chengdu, 611731, P. R. China. E-mail: tang@uestc.edu.cn; tanghui@uestc.edu.cn

† Electronic supplementary information (ESI) available. See DOI: https://doi.org/10.1039/d4ra04421e

carbon layer provides conductive network for fast electron transfer. As a result, the LTO@C exhibits a high reversible capability of 228.8 mA h g^{-1} at 10C and demonstrates good cycling performance, retaining 71.7% of its capacity after 1000 cycles at 10C. This work presents a promising approach for the preparation of binder-free, high-power performance LTO/C anodes.

Experimental

Materials preparation

Synthesis of TiO_2 nanotube arrays. Typically, TiO_2 nanotube arrays are fabricated by the anodization using 0.1 M NH_4F in 3 : 97 (v/v) mixture of ethylene glycol and water as the electrolyte. A 0.5 mm thick titanium foil was firstly ground with sandpaper to remove surface oxides. The smooth Ti foil is then used as working electrode, and graphite is used as counter electrode with a voltage of 40 V applied for 3 hours to fabricate the nanotube arrays. The distance between the electrodes is maintained at 3 cm. After anodization, the sample is rinsed extensively with deionized water and dried in a vacuum oven.

Synthesis of TiO_2 nanotube arrays. The LTO/C samples were prepared through a hydrothermal approach followed by a calcination process. Briefly, 2.4 g LiOH and 1.5 g glucose were mixed in 15 mL of deionized water to form the precursor solution. Then, the 3 × 3 cm Ti foil with TiO_2 nanotube arrays on its surface and the precursor solution were added into 25 mL Teflon-lined stainless autoclave and kept in an oven at 180 °C for 8 h. The foil was then annealed at 550 °C for 2 h under a nitrogen atmosphere. The synthesis process of LTO is almost identical to that of LTO@C, except for not adding glucose as a carbon source (Scheme 1).

Materials preparation. The structure and composition of the prepared materials were identified using X-ray diffraction (XRD) with Cu Kα radiation, and the valence states research were investigated using X-ray photoelectron spectroscopy (XPS, Thermo Scientific K-Alpha). The morphology and architecture of the prepared materials were characterized by Field Emission Scanning Electron Microcopy, (FESEM, Merlin Compact) and transmission electron microscopy (TEM, Tecnai G2 F30).

Electrochemical measurement. The obtained LTO and LTO@C were directly assembled as anodes of LIBs without any binder or conductive agent. Then the two electrodes were assembled in an Ar-filled glove box and used as the working electrode. Li foil was used as the counter electrode, 1 M LiPF6 in ethylene carbonate (EC)/diethyl carbonate (DEC) (v/v) was used as the electrolyte. Galvanostatic charge–discharge (GCD) and rate performance tests were carried out at 25 °C on a CT-ZWJ-4′S-T-1 U battery testing system with the cut-off voltages of 1.0 and 3.0 V. Cyclic voltammetry (CV) was performed on a CHI 660 electrochemical workstation.

Results and discussion

The XRD pattern of LTO@C nanotube arrays is illustrated in Fig. 1a, the diffraction peaks at 18.4°, 35.6°, 43.3° and 62.8° correspond to the (111), (311), (400) and (440) planes of the cubic spinel LTO phase (JCPDS No. 49-0207), indicating the successfully synthesized of LTO. Additionally, the halo peak at 20–30° belongs to the (002) plane of graphite carbon (JCPDS No. 89-8487), which confirmed the doping of carbon. And the peaks at 38.2°, 39.9°, 52.9°, 70.7°, and 76.0° can be assigned to the Ti foil substrate.

Furthermore, the sharp and intense peaks with no impurity peaks confirm the high crystallinity and high purity of the LTO@C samples. Fig. 1b shows the Raman spectra of LTO@C, the peaks were observed at 1340 cm^{-1} and 1600 cm^{-1}. These peaks represent D band and G band of carbon, respectively. And the intensity ratio of D band and G band (I_D/I_G) is 0.83, indicating good graphitization which can facilitate electron transfer.[25,26]

A thermogravimetric (TG) analysis was conducted under a nitrogen atmosphere to investigate the carbon content. As shown in Fig. S1,† the analysis revealed that from room temperature to 500 °C, the mass of LTO@C underwent a continuous decline, indicating the presence of volatile components. Beyond 500 °C, the mass remained stable, indicating the completion of the decomposition process. The total mass loss of 17.25% is attributed to the carbon content present in the sample.

The morphology of as-prepared samples is characterized using SEM. As shown in Fig. 2a, the TiO_2 nanotubes are uniformly distributed on the substrate with a thickness of 80–100 nm and smooth surface morphology. In contrast to the smooth surface of TiO_2 substrate, the appearances of LTO and LTO@C became much rougher (Fig. 2b and c). The SEM image after 1000 cycles at 1C is shown in Fig. 2d, which appears rougher than before, with some tubes are filled with particles. Nonetheless, the morphology is well retained, indicating good stability of LTO@C. Moreover, the nanotube arrays have been preserved after the hydrothermal and annealing processes. The obvious nanotube arrays structure can also be observed in TEM

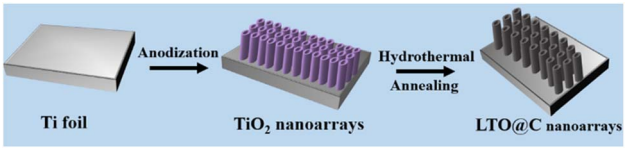

Scheme 1 Schematic illustration of the synthesis process of LTO@C nanoarrays.

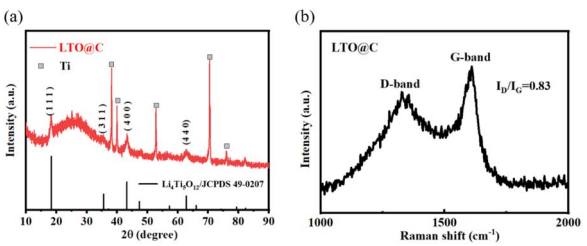

Fig. 1 XRD pattern and Raman spectra of LTO@C. (a) the XRD pattern, and (b) the Raman spectra.

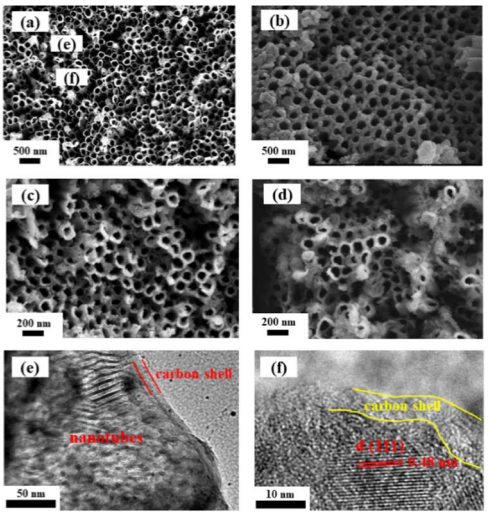

Fig. 2 SEM results of (a) TiO_2, (b) LTO, (c) LTO@C and (d) LTO@C after 1000 cycles; (e and f) TEM results of LTO@C.

image (Fig. 3e), and the appearance of carbon shell indicates the formation of a carbon coating. The corresponding HRTEM image (Fig. 3f) also shows a carbon shell with a thickness of 3–5 nm, and the lattice spacing of 0.48 nm corresponds to the (111) plane of $Li_4Ti_5O_{12}$.

XPS was performed to investigate the surface chemical state of the LTO@C sample. The wide-survey XPS spectra (Fig. 3a) reveals the presence of Ti, O, and C elements. The high-resolution C 1s spectra (Fig. 3b) shows two peaks at 284.8 eV and 289.8 eV, corresponding to sp^2-hybridized graphitic carbon and oxygen bridged C, respectively. The high-resolution Ti 2p spectra is shown in Fig. 3c. Two peaks at 464.9 eV and 459.2 eV correspond to the Ti $2p^{1/2}$ and Ti $2p^{3/2}$ of Ti^{4+} is observed. Additionally, the spectra of O 1s (Fig. 3d) shows two peaks at 529.6 eV and 531.5 eV, indicating the formation of Ti–O and Ti–O–C bond.

The electrochemical testing results of LTO and LTO@C samples are shown in Fig. 4. The charging–discharging curves (Fig. 4a) in the first cycle at 1C of LTO@C exhibit an obviously flat charging and discharging voltage platform around 1.43 V,

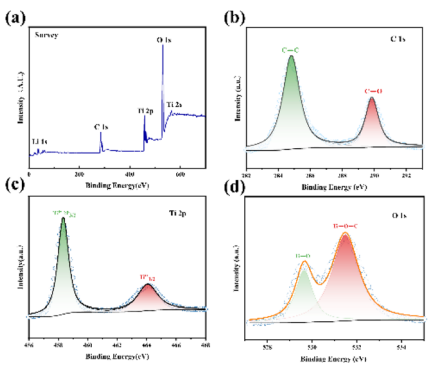

Fig. 3 XPS results of LTO@C: (a) wide-survey; (b) C 1s spectra; (c) Ti 2p spectra; (d) O 1s spectra.

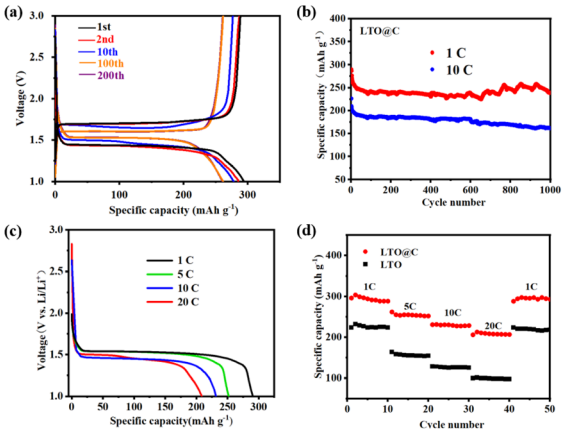

Fig. 4 (a) Charge–discharge curves of LTO@C at 1C of different cycles; (b) reversible capacity *vs.* cycles of LTO@C at different current densities. (c) Cycling performance at of LTO@C at 1C, 5C, 10C and 20C; (d) rate performance of LTO and LTO@C.

and the initial coulomb efficiencies of LTO@C is 97.9%. The second cycle shows similar capacity with no obvious decrease. Notably, after 200 cycles at 1C, the LTO@C retains a high capacity of 260 mA h g^{-1}. The excellent cycling stability is also proved by charging and discharging cycles at different current densities. As shown in Fig. 4b, the LTO@C retains 86.6% of its initial capacity after 1000 cycles at 1C and 71.7% at 10C. Fig. 4c shows the capacity of LTO@C at 1C, 5C, 10C and 20C is 290, 251.9, 228.8 and 208.7 mA h g^{-1}, respectively. Furthermore, in Fig. 4d, the discharge specific capacity of LTO@C is significantly better than that of LTO, even the capacity of LTO@C at 20C (206 mA h g^{-1}) is close to that of LTO at 1C (224 mA h g^{-1}). In addition, LTO@C exhibits good rate performance, as the capacity of LTO@C reduces slowly with the increase of current density, and when back to 1C, its capacity can return to the initial level. This can be attributed to the enhanced Li^+ transfer by the specially designed nanotube structure and the improved electron conductivity owing to carbon shell coating.[19]

Fig. 5 shows the first three cyclic voltammetry cycles of LTO and LTO@C, respectively. It can be seen that both the two samples have a pair of redox peaks in the process of charge and discharge, indicating the process of Li^+ insertion (reduction peak) and extraction (oxidation peak) in LTO, respectively. Moreover, the voltage differences between oxidation peak and reduction peak are 0.49 V and 0.39 V for LTO and LTO@C, respectively. The smaller voltage difference of LTO@C means

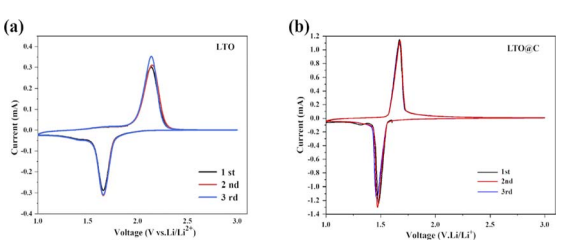

Fig. 5 CV curves of (a) LTO and (b) LTO@C.

lower polarization effect, which can be attribute to the uniform nanotube structure and carbon shell coating.

Conclusions

In summary, core–shell structured LTO@C combined nanotube arrays structure and a carbon coating shell has been synthesized by anodization followed by a hydrothermal reaction with lithium hydroxide and glucose as a lithium source and inexpensive carbon source, respectively. The prepared typical LTO@C retains the special nanotube structure of TiO_2 with a size of 80–100 nm, and the thickness of the carbon shell on the LTO surface is about 3–5 nm. Compared to the LTO without carbon coating layers, LTO@C exhibits much better specific capacity and rate performance. Even the capacity of LTO@C at 20C (206 mA h g^{-1}) is close to that of LTO at 1C (224 mA h g^{-1}). LTO@C also has excellent stability, after 1000 cycles at 10C, the discharge specific capacity still retains 71.7% of 164 mA h g^{-1}. The uniform nanotube arrays morphology and improved conductivity from the carbon layer are assumed to contribute to the improved rate performance of the LTO@C sample.

Data availability

All data presented in this manuscript can be provided by the corresponding author on reasonable demand.

Conflicts of interest

There are no conflicts to declare.

Acknowledgements

This research was supported by the National Key Research and Development Project (Grant No. 2020YFB1506001), Sichuan Province Science and Technology Support Program (Grant No. 2021YFG0231, 2022YFG0258)

Notes and references

1 M. Yuan, H. Liu and F. Ran, *Mater. Today*, 2023, **63**, 360–379.
2 Q. Liu, G. Zhu, R. Li, S. Lou, H. Huo, Y. Ma, J. An, C. Cao, F. Kong, Z. Jiang, M. Lu, Y. Tong, L. Ci, G. Yin and J. Wang, *Energy Stor. Mater.*, 2021, **41**, 1–7.
3 H. Liu, Z. Zhu, Q. Yan, S. Yu, X. He, Y. Chen, R. Zhang, L. Ma, T. Liu, M. Li, R. Lin, Y. Chen, Y. Li, X. Xing, Y. Choi, L. Gao, H. S. Y. Cho, K. An, J. Feng, R. Kostecki, K. Amine, T. Wu, J. Lu, H. L. Xin, S. P. Ong and P. Liu, *Nature*, 2020, **585**, 63–67.
4 Y. Wu, W. Wang, J. Ming, M. Li, L. Xie, X. He, J. Wang, S. Liang and Y. Wu, *Adv. Funct. Mater.*, 2018, **29**, 1805978.
5 J. Liu, K. Song, P. A. van Aken, J. Maier and Y. Yu, *Nano Lett.*, 2014, **14**, 2597–2603.
6 L. Shen, H. Li, E. Uchaker, X. Zhang and G. Cao, *Nano Lett.*, 2012, **12**, 5673–5678.
7 M. Gockeln, S. Pokhrel, F. Meierhofer, J. Glenneberg, M. Schowalter, A. Rosenauer, U. Fritsching, M. Busse, L. Mädler and R. Kun, *J. Power Sources*, 2018, **374**, 97–106.
8 G. Xu, Y. Tian, X. Wei, L. Yang and P. K. Chu, *J. Power Sources*, 2017, **337**, 180–188.
9 E. Kang, Y. S. Jung, G. H. Kim, J. Chun, U. Wiesner, A. C. Dillon, J. K. Kim and J. Lee, *Adv. Funct. Mater.*, 2011, **21**, 4349–4357.
10 N. Cao, Z. Song, Q. Liang, X. Gao and X. Qin, *Electrochim. Acta*, 2017, **235**, 200–209.
11 Q. Cheng, S. Tang, J. Liang, J. Zhao, Q. Lan, C. Liu and Y. C. Cao, *Results Phys.*, 2017, **7**, 810–812.
12 A. Lakshmi-Narayana, M. Dhananjaya, C. M. Julien, S. W. Joo and C. V. Ramana, *ACS Appl. Mater. Interfaces*, 2023, **15**, 20925–20945.
13 H. J. Hong, S. Y. Lee, S. Kwon, B. S. Kim, S. Yoon and I. S. Park, *J. Alloys Compd.*, 2021, **886**, 161296.
14 K. Zhou, X. Fan, W. Chen, F. Chen, X. Wei, A. Li and J. Liu, *Electrochim. Acta*, 2017, **247**, 132–138.
15 Z. Yao, X. Xia, C. A. Zhou, Y. Zhong, Y. Wang, S. Deng, W. Wang, X. Wang and J. Tu, *Advanced Science*, 2018, **5**, 1700786.
16 J. Gong, X. Zeng, X. Zhou, R. Shi, K. Xia and K. Huang, *J. Electroanal. Chem.*, 2024, **952**, 117932.
17 F. Zhang, F. Yi, T. Meng, A. Gao, D. Shu, H. Chen, H. Cheng and X. Zhou, *ACS Sustain. Chem. Eng.*, 2018, **7**, 916–924.
18 S. Luo, P. Zhang, T. Yuan, J. Ruan, C. Peng, Y. Pang, H. Sun, J. Yang and S. Zheng, *J. Mater. Chem. A*, 2018, **6**, 15755–15761.
19 X. Li, X. Huang, Y. Chen, J. Mei, W. Xu, L. Wang and D. L. Peng, *Electrochim. Acta*, 2021, **390**, 138874.
20 N. Sergienko, E. C. Lumbaque, N. Duinslaeger and J. Radjenovic, *Appl. Catal., B*, 2023, **334**, 122831.
21 L. Gan, Y. Wu, H. Song, C. Lu, S. Zhang and A. Li, *Chemosphere*, 2019, **226**, 329–339.
22 P. Zhang, S. Zhu, Z. He, K. Wang, H. Fan, Y. Zhong, L. Chang, H. Shao, J. Wang, J. Zhang and C.-N. Cao, *J. Alloys Compd.*, 2016, **674**, 1–8.
23 W. Ji, W. Li, T. C. Zhang, Y. Wang and S. Yuan, *Sep. Purif. Technol.*, 2023, **312**, 123370.
24 D. Mu, Y. Chen, B. Wu, R. Huang, Y. Jiang, L. Li and F. Wu, *J. Alloys Compd.*, 2016, **671**, 157–163.
25 Z. Zhu, F. Cheng and J. Chen, *J. Mater. Chem. A*, 2013, **1**, 9484–9490.
26 B. Yue, L. Wang, N. Zhang, Y. Xie, W. Yu, Q. Ma, J. Wang, G. Liu and X. Dong, *Small*, 2023, **20**, 2308603.